First Results from the CHARA Array. IV. The Interferometric Radii of Low-Mass Stars

D. H. Berger[1]

The CHARA Array, Mount Wilson Observatory, Mount Wilson, CA 91023

berger@chara-array.org

D. R. Gies, H. A. McAlister

Center for High Angular Resolution Astronomy, Georgia State University, P.O. Box 3969, Atlanta, GA 30302-3969

gies@chara.gsu.edu, hal@chara.gsu.edu

T. A. ten Brummelaar

The CHARA Array, Mt. Wilson Observatory, Mt. Wilson, CA 91023

theo@chara-array.org

T. J. Henry

Center for High Angular Resolution Astronomy, Georgia State University, P.O. Box 3969, Atlanta, GA 30302-3969

thenry@chara.gsu.edu

J. Sturmann, L. Sturmann, N. H. Turner

The CHARA Array, Mt. Wilson Observatory, Mt. Wilson, CA 91023

judit@chara-array.org, sturmann@chara-array.org, nils@chara-array.org

S. T. Ridgway, J. P. Aufdenberg

National Optical Astronomy Observatory, P.O. Box 26732, Tucson, AZ 85726

ridgway@noao.edu, jasona@noao.edu

and

A. Mérand

LESIA, UMR8109, Observatoire de Paris-Meudon, 5 place Jules Janssen, 92195 Meudon Cedex, France

antoine.merand@obspm.fr

ABSTRACT

We have measured the angular diameters of six M dwarfs with the CHARA Array, a long-baseline optical interferometer located at Mount Wilson Observatory. Spectral types range from M1.0 V to M3.0 V and linear radii from 0.38 to 0.69 $R_{\odot}$. These results are consistent with the seven other M-dwarf radii measurements from optical interferometry and with those for sixteen stars in eclipsing binary systems. We compare all directly measured M dwarf radii to model predictions and find that current models underestimate the true stellar radii by up to 15-20%. The differences are small among the metal-poor stars but become significantly larger with increasing metallicity. This suggests that theoretical models for low mass stars may be missing some opacity source that alters the computed stellar radii.

Subject headings: infrared: stars — instrumentation: high angular resolution — instrumentation: interferometers — stars: radii — stars: late-type — stars: individual (GJ 15A, GJ 514, GJ 526, GJ 687, GJ 752A, GJ 880)

1. Introduction

Cool, low-mass stars dominate the stellar census (Henry et al. 1997; Reid et al. 2004), yet they remain elusive and enigmatic objects. Because of their small size and cool surface temperature, nearby members of our solar neighborhood are still being discovered via proper motion surveys (Hambly et al. 2004; Lépine 2005; Subasavage et al. 2005) and parallaxes are being determined for these new stellar neighbors (Jao et al. 2005; Costa et al. 2005). Furthermore, the low-mass stars we do know about are not well understood. Their fundamental properties are difficult to measure and do not adequately constrain atmospheric and interior stellar models. In addition to effective temperature and mass, the size of field stars at the cool end of the main sequence is arguably one of the most difficult properties to determine.

[1]present address: University of Michigan, Dept. of Astronomy, 500 Church St., 917 Dennison Bldg., Ann Arbor, MI 48109-1042

There are currently only two methods to measure directly the stellar radii of cool dwarfs: light curve and radial velocity studies of double-lined eclipsing binaries and long-baseline interferometry of single stars. The former method is biased toward main sequence stars larger than the Sun (Andersen 1991), and the latter toward brighter and larger giants and supergiants. Within the past ten years, cooler and smaller stars are being added to the database of stars with known fundamental properties. There are sixteen known M-dwarfs that are members of eclipsing binaries for which we have have stellar radii: both components of GJ 2069A (Delfosse et al. 1999), both components of CM Dra (Lacy 1977; Metcalfe et al. 1996), both components of CU Cnc (Ribas 2003), both components of YY Gem and one component of V818 Tau (Torres & Ribas 2002), both components of BW3 V38 (Maceroni & Montalbán 2004), one component of RXJ2130.6+4710 (Maxted et al. 2004), both components of TrESHer0-07621 (Creevey et al. 2005), and both components of GU Boo (López-Morales & Ribas 2005). From long-baseline optical interferometry, the situation is more bleak as there heretofore were only seven M dwarfs (GJ 15A, GJ 191, GJ 205, GJ 411, GJ 551, GJ 699, and GJ 997) for which stellar radii have been measured (Lane et al. 2001; Ségransan et al. 2003).

Here we report on measurements of the angular diameters of six M dwarfs. We obtained these measurements from observations made with the Center for High Angular Resolution Astronomy (CHARA) Array, a 6-element optical/near-infrared interferometer located at Mount Wilson Observatory, California. From these measurements, we deduce the linear sizes and further refine the mass–radius relation. In addition, we calculate their surface gravities and effective temperatures. This paper is the fourth in a series of commissioning science observations with the CHARA Array. The other three papers vary in topic from the rapid rotators Regulus (McAlister et al. 2005) and Alderamin (van Belle et al. 2006) to an overview of the CHARA Array (ten Brummelaar et al. 2005).

2. Observations

The majority of observations were completed in 2004 June, while others were mixed into the standard queue observing throughout the end of 2003 and most of 2004. All observations were made using the K' filter ($\lambda_0 = 2.13\ \mu$m, $\Delta\lambda = 0.35\ \mu$m; note that the central wavelength for the filter alone differs slightly from the system effective wavelength adopted by McAlister et al. 2005, but the difference has a negligible effect on our results). Data for GJ 15A were obtained using the most western and eastern telescopes (W1 and E1, respectively) and for GJ 880 using the inner southern telescope (S2) and W1. The data for the remaining targets were observed with the most southern telescope (S1) and E1. The maximum baseline separations

between these telescopes are 314 meters for W1-E1, 249 meters for S2-W1, and 331 meters for S1-E1. In these configurations, angular diameters as small as 0.5 milliarcsecond (mas) can readily be measured at the K' spectral band.

Targets were chosen from the Gliese and Jahreiß catalog (Gliese & Jahreiß 1991) based on color ($B-V>1$) and distance (parallax $\pi > 100$ mas) such that their predicted angular size exceeded 0.4 mas. Targets also had to be within the detection limits of the instrument ($B < 11$ for tip-tilt correction, $V < 10$ for image acquisition, and $K' < 6$ for the near-IR detector). Table 1 is a summary of the observations for this paper. Column 1 is the Gliese and Jahreiß catalog designation, column 2 is the Luyten Half-Second (LHS) Catalog designation (Luyten 1979), column 3 gives the name of the calibrator star, column 4 indicates the telescope pair (and baseline) used, column 5 gives the UT observation date, and column 6 gives the number of observations.

Measurements of all but GJ 15A were taken using the "CHARA Classic" beam combiner. It is a two-beam, pupil-plane (or Michelson) combiner utilizing path length modulation; details of the instrumentation and configuration are given by Sturmann et al. (2003). GJ 15A was observed with FLUOR, a single-mode fiber beam combiner designed by collaborators at the Paris Observatory (Coudé du Foresto et al. 2003), because it was the available instrument at the time and the target was within its sensitivity limits. The calibrator for GJ 15A was HD 2952, and was chosen from the "Calibrator Stars for 200m Baseline Interferometry"[2] catalog (Mérand et al. 2005), which includes corrections for limb darkening. While FLUOR benefits from spatially cleaned beams, the "CHARA Classic" beam combiner has greater sensitivity. Hence the two instruments complement each other in this respect.

The same near-IR detector was at the back end of each beam combiner. The fringe sampling frequency was either 100 or 150 Hz, depending on the seeing conditions and source brightness. For the same reasons, either 1 or 2×2 pixels were read out. The camera readout was adjusted to maintain five samples per fringe. Each merged data scan from "CHARA Classic" was formed from 200 scans with photometric calibration scans made before and after. Photometric calibration scans for FLUOR are performed during the scan on separate fiber channels.

Atmospheric and instrumental coherence losses were estimated by interleaving measurements of unresolved stars or stars with known angular diameters. Calibrators were chosen using the *gcWeb* utility available online from the Michelson Science Center[3]. We restricted

[2]http://vizier.hia.nrc.ca/viz-bin/Cat?J/A%2bA/433/1155

[3]http://mscweb.ipac.caltech.edu/gcWeb/gcWeb.jsp

our selection to main sequence stars with estimated angular sizes less than 0.4 mas, which yields visibility amplitudes greater than 90% when measured with the S1-E1 baseline in the K'-band. The calibrator observations were in close proximity on the sky (within 10°) and in time (within 30 minutes) to each source observation. The typical duty cycle from the start of one observation to the start of the next was approximately 10 minutes.

3. Data Reduction

The reduction algorithms developed for data from the CHARA Array are described in detail by ten Brummelaar et al. (2005). We employed a commonly used technique of integrating the power of each fringe scan (Benson et al. 1995), but we removed the variance term resulting from atmospheric turbulence. The resulting quantity is the visibility amplitude ($\mathcal{V}$), and not the more common $\mathcal{V}^2$. Data from GJ 15A and its calibrator were analyzed by methods specific to the FLUOR instrument (Coudé du Foresto et al. 1997; Perrin 2003) and the following description does not pertain.

The calibrated visibility amplitude of the science object ($\mathcal{V}_o$) was calculated using the relation

$$\mathcal{V}_o = \frac{1}{\eta}\mathcal{V}'_o \tag{1}$$

where η is the interferometer's efficiency and $\mathcal{V}'_o$ is the instrumental visibility amplitude of the science object as measured on the sky. By interleaving measurements of a calibrator of known angular size and thus a known calibrated visibility amplitude, one can measure η via the ratio of the instrumental to calibrated visibility amplitude, or $\eta = \mathcal{V}'_c/\mathcal{V}_c$. Furthermore, if the calibrator is unresolved, $\mathcal{V}_c$ is unity, and η is measured directly. However, the high resolution at long baselines and instrument sensitivity limitations significantly reduce the number of available unresolved sources, especially within close proximity to the science object. Therefore, we were left to use slightly resolved calibrators and to determine $\mathcal{V}_c$ through other means.

3.1. Angular Diameters of the Calibrators

From conservation of energy, the true limb-darkened angular diameter of a star ($\theta_{\rm LD}$) is related to ratio of the stellar flux reaching the top of the Earth's atmosphere ($F_\lambda^\oplus$) at wavelength λ to the flux leaving the stellar surface ($F_\lambda^\star$):

$$\frac{\theta_{\rm LD}^2}{4} = \frac{F_\lambda^\oplus}{F_\lambda^\star}. \tag{2}$$

$F_\lambda^\star$ is determined from stellar model atmospheres and $F_\lambda^\oplus$ from extinction-corrected photometry and absolute spectrophotmetry. This was an idea first proposed by Gray (1967) and later refined by Blackwell & Shallis (1977). A potential source of error in $F_\lambda^\star$ is the uncertainty in determining the correct input parameters for the model atmosphere. For example, if the effective temperature ($T_{\rm eff}$), metallicity ([Fe/H]), and/or surface gravity ($\log g$) are not well known, there can be difficulty in choosing the correct model. As pointed out by Blackwell & Shallis, the infrared region is less sensitive to model input approximations than the visible — hence the method to derive angular diameters from infrared photometry is known as the InfraRed Flux (IRF) method. Because our observations were obtained in the K'-band, our derived radii measurements are relatively unaffected by problems related to limb darkening and/or absorption line contamination.

We selected model atmospheres from Kurucz (1992) and linearly interpolated the fluxes between $T_{\rm eff}$ grid points. We adopted $\log g = 4.5$, which is appropriate for mid-temperature dwarf stars, and assumed the metallicity to be solar. However, changing $\log g$ and/or the metallicity did not significantly effect the resulting $\theta_{\rm LD}$. The Two Micron All Sky Survey (2MASS) point source catalog (Cutri et al. 2003) provided the near-IR broad-band photometry data, which were then transformed to fluxes (Cohen et al. 2003). A weighted fit of the 2MASS photometry to the model flux yielded angular diameters less than 0.4 mas and typical errors of 4-5% (Figure 1). For calibrators with such small angular size, the propagated fractional error in the target angular diameter is much lower than this percentage (van Belle & van Belle 2005). We list the names and adopted parameters of the calibrator stars in Table 2, and our derived $\theta_{\rm LD}$ values are given there in column 5.

The IRF method yields $\theta_{\rm LD}$. However, it is common practice to fit a visibility function for a uniform disk angular diameter ($\theta_{\rm UD}$), which is given by

$$\mathcal{V} = \left| \frac{2J_1\left(\pi B \theta_{\rm UD}/\lambda_0\right)}{\pi B \theta_{\rm UD}/\lambda_0} \right| \tag{3}$$

and depends on the projected baseline (B) and the effective wavelength (λ_0). In order to compute the efficiency (η) from the measured visibility of the calibrator ($\mathcal{V}_c'$), we need to transform $\theta_{\rm LD}$ into an equivalent $\theta_{\rm UD}$ that has the same visibility amplitude at the observed projected baseline and wavelength. To do this, we calculated a correction factor ($\rho_w = \theta_{\rm LD}/\theta_{\rm UD}$) based on $T_{\rm eff}$, metallicity (Nordstrom et al. 2004), and the transmission of the K'-filter (Davis et al. 2000; Tango & Davis 2002). These correction factors (Table 2, column 6) result in slightly smaller ($\approx 1.5\%$) diameters for equivalent uniform disks.

3.2. Calibrated Visibility Amplitudes

Because calibrator measurements were not made simultaneously with object measurements, we linearly interpolated in time between the values of $\mathcal{V}_c'$ immediately before and after each $\mathcal{V}_o'$. We then used the calibrator $\theta_{\rm UD}$ and the known values of B and λ_0 to compute $\mathcal{V}_c$. From $\mathcal{V}_c'$ and $\mathcal{V}_c$, we determined the instrumental efficiency (η) for visibility measurement. Typically values of η ranged from 40 to 50% and varied by only a few percent over the course of the night. This can be attributed to the stability of the system and habitual realignment of the optics before every observation. Finally, from eq. 1, we determined the calibrated visibility amplitudes ($\mathcal{V}_o$). Table 3 lists the Modified Julian Dates (MJD), projected baselines, and visibility amplitudes (with error estimates) associated with the mid-point time of observation for each dwarf star. Errors in calibrator angular size (§3.1) and visibility amplitudes were propagated to the calibrated visibility amplitude error estimates.

4. Angular Diameters and Radii

We can determine the stellar radius from the angular diameter and parallax in two ways. First, we can assume that the stars are uniform disks and then fit the fringe visibility as a function of baseline using eq. 3. This estimate of $\theta_{\rm UD}$ is given in column 2 of Table 4. However, we know that real stars are limb darkened (by a small amount in the K'-band), so that their actual, limb darkened diameters will be slightly larger than the uniform disk diameters (see Table 2). In principle, it is no harder to fit a limb darkened visibility curve to the observations (Davis et al. 2000, eq. 6), but to do so we first need to establish the stellar parameters in order to obtain the appropriate K'-band limb darkening law from stellar atmosphere models.

We approached this problem as follows. Claret (2000) has tabulated limb darkening coefficients for the near-IR that are based upon solar metallicities. We chose the coefficients calculated using the PHOENIX code for modeling stellar atmospheres (Table 38 from Claret 2000). The limb darkening relations are listed as functions of $T_{\rm eff}$ and $\log g$. We can determine these parameters using an iterative scheme that is based upon sequential improvements in the radius estimate. We start with a stellar radius estimate derived from the uniform disk angular diameter (column 2 of Table 4) and the parallax from the NStars database[4]. NStars parallaxes are the weighted means of all currently available parallaxes, including those of Hipparcos and the Yale Parallax Catalog. Then we use the Stefan-Boltzmann relation to find

[4]http://nstars.nau.edu

$T_{\rm eff}$ from the bolometric luminosity and radius. We determined the bolometric luminosity from the absolute K magnitude using a bolometric correction based on the $I-K$ color index (derived from spectral energy distribution fits of M-stars by Leggett et al. 2000). We used absolute K magnitudes calculated from NStars parallaxes and 2MASS K magnitudes and $I-K$ color indices from Leggett (1992) to find the luminosities given in column 5 of Table 4, which were then used to find $T_{\rm eff}$ from the assumed stellar radius. We adopted $L_{\odot} = 3.86 \times 10^{33}$ erg s^{-1} and $M_{bol\odot} = 4.75$ in this calculation, and the scatter in the bolometric correction relation results in a luminosity error of ± 0.022 dex. Next we used estimates of the stellar mass (column 4 of Table 5) with the assumed radius to find $\log g$. Stellar masses were estimated using the K-band mass–luminosity relation of Delfosse et al. (2000), which have a typical error of $\pm 10\%$. With $T_{\rm eff}$ and $\log g$ set, we then found the limb darkening law from Claret (2000) and made a least-squares error-weighted fit of the limb-darkened visibility curve to the observations to obtain the limb darkened angular size $\theta_{\rm LD}$.

We repeated the process and revised the temperature and gravity estimates by estimating a new radius from $\theta_{\rm LD}$ and parallax, and then fitted the visibilities again with the revised limb darkened visibility curve. In practice this procedure converged (with negligible parameter differences between iterations) in only two iterations because the IR limb darkening is only slightly different from a uniform disk and is relatively insensitive to the adopted temperature and gravity. In fact, a 1-σ change in the adopted temperature and gravity has no detectable effect on $\theta_{\rm LD}$. Our final values of $\theta_{\rm LD}$, reduced chi-squared ($\chi^2_{\rm red}$), stellar radius, $T_{\rm eff}$, and $\log g$ are listed in Table 4 and the fitted, limb darkened visibility curves are plotted with the observations in Figure 2. The fractional errors in the derived temperatures are approximately one half the fractional errors in the radii or about 3%, and the errors in $\log g$ amount to approximately ± 0.07 dex (as derived from the errors in fractional mass and radius). Changing these parameters by one standard deviation does not effect the radius determinations at the precision we are reporting them.

The one inconsistency in this method is that we have relied on the solar abundance atmospheric models from Claret (2000) to estimate the limb darkening, while some of our targets are somewhat metal poor (column 3, Table 5). It will be interesting to revisit our calculations when limb darkening results for metal poor atmospheres are eventually developed, but we doubt that our radius results will change significantly because the limb darkening corrections are small.

We found that the values of $\chi^2_{\rm red}$ (given in column 4 of Table 4) exceeded the expected value of unity for all the targets except GJ 15A and GJ 880 (the small value for GJ 15A probably results from our sample of two measurements). Thus, the internal visibility am-

plitude errors associated with an individual data set underestimate the full error budget, and consequently, we used the observed scatter from the fits to rescale the minimum, best-fit value of $\chi^2_{\rm red}$ to unity. We added a 6% noise floor to account for the night-to-night fluctuation in angular diameter measurement, as calculated from objects with multi-night observations. This term was added in quadrature to the statistical error. We show in Figure 3 the distribution of the fractional deviations from the fit for GJ 752A, the target with the most observations. We also plot a linear regression fit of the residuals that has a non-zero slope which is set by a few outlying points from two nights (2004 June 13-14). The 6% noise floor also accounts for this slight linear trend seen in these commissioning observations.

We also determined effective temperatures by a direct comparison of the observed and predicted fluxes in the K-band based upon the observed angular diameters. We used the 2MASS K_s band magnitudes and the adopted flux zero-point from Cohen et al. (2003) to form the following relation:

$$K_s = -2.5 \log F_\lambda - 5 \log \theta_{LD} + 17.157 \tag{4}$$

where F_λ is the model flux (erg cm^{-2} s^{-1} Å^{-1}) averaged over the 2MASS K_s filter response (Cohen et al. 2003) and $\theta_{\rm LD}$ is the limb-darkened angular diameter (mas). The model fluxes were taken from the PHOENIX atmosphere code of Brott & Hauschildt (2005)[5] and these are primarily functions of effective temperature (although we did interpolate in these models for the appropriate gravity and metallicity of each target). We used our values of $\theta_{\rm LD}$ from Table 4 to find the estimates of $F_\lambda(T_{\rm eff})$ and hence effective temperature that are listed in column 8 of Table 4 (under the heading $T_{\rm eff}$(2MASS)). The temperatures agree well with those from the bolometric correction method, $T_{\rm eff}$(BC), discussed above. Note that the adopted limb-darkened diameters themselves depend on the assumed temperature through the limb darkening coefficients, but since the resulting temperatures are so similar and the limb darkening is a minor effect, this approximation has a negligible impact on the temperature derived this way.

Finally we note that we find no evidence in our data that any target has a close binary companion that could affect the radius estimates. The targets are all radial velocity constant (r.m.s. < 100 m s^{-1}) according to the spectroscopic survey of Nidever et al. (2002). Optical speckle interferometry by McAlister et al. (1987) and Balega et al. (1999) indicates that GJ 687 has a companion at a separation of $0\farcs3$, which is too wide to influence our observations (except as a source of incoherent light that might reduce the measured visibility). However, near-infrared speckle observations (Leinert et al. 1997) and high resolution HST/NICMOS

[5]ftp://ftp.hs.uni-hamburg.de/pub/outgoing/phoenix/GAIA/

imaging (T. J. Henry, private communication) show no evidence of a companion at such a separation. We examined the mean fringe envelopes for each set of scans of this star and found no detectable companion with $\Delta K_s < 2$ in the separation range 12 – 70 mas. Clearly more observations are required to settle the question about a companion to GJ 687, but we tentatively assume that the measured visibility is dominated by the photospheric disk of the bright M-dwarf.

5. Mass–Radius Relation

In an effort to further constrain the poorly populated mass–radius relation for low-mass stars, we started by comparing our results with other low-mass stellar radii directly measured with long-baseline interferometers (Lane et al. 2001; Ségransan et al. 2003). All masses were derived from the same K-band mass–luminosity relation of Delfosse et al. (2000), and we adopted a 10% error to account for photometric and empirical fitting errors. Note that the mass derived from the absolute K magnitude should have little or no dependence upon the stellar metallicity (see Fig. 3b of Baraffe et al. 1998). Lane et al. (2001) also measured the angular diameter of GJ 15A and their value of $\theta_{\rm UD} = 0.985 \pm 0.05$ mas agrees with our value $\theta_{\rm UD} = 0.976 \pm 0.016$ mas. However, we adopted a less severe limb-darkening correction resulting in a smaller linear diameter. In our mass–radius plot (Figure 4), we only show our data point for GJ 15A. Eclipsing binary star measurements are also shown in Figure 4 as open circles, and it should be noted that some of the errors bars are smaller than the symbol size. The theoretical models of Chabrier & Baraffe (1997) for [M/H] = 0, −0.5, and −1.0 are shown as the lines. Additionally, the models of Siess et al. (1997) for [M/H] = 0, −0.3 (assuming $Z_\odot = 0.02$) are plotted to show the range of model uncertainty. According to these models, metallicity should have little effect on radius for a given mass star. However, there is either a systematic effect in the data or the models are underestimating the sizes of the stars for a given mass. We doubt the former possibility because this effect is seen in data from multiple instruments and is present in both the interferometric and binary results. Indeed, the larger than expected radii have already been noted in several investigations (Leggett et al. 2000; Ségransan et al. 2003; López-Morales & Ribas 2005).

Mullan & MacDonald (2001) argue that larger radii could result from pervasive magnetic fields that could alter the interior structure and push the occurrence of completely convective interiors to stars of lower effective temperatures. They suggest that M-stars with active magnetic fields will have larger radii than predicted by standard models. However, there is no evidence that the M-dwarfs in our sample have any special magnetic properties. All are slow rotators (Delfosse et al. 1998), have moderate X-ray coronal emission (Schmitt et

al. 1995; Hünsch et al. 1999), have normal chromospheric Hα lines (Gizis et al. 2002), and show no evidence of photometric variability in *Hipparcos* photometry (Perryman et al. 1997). Thus, these stars do not have the exceptionally strong magnetic fields that would lead to larger radii according to the models of Mullan & MacDonald.

On the other hand, our sample stars do span a significant range in metallicity, and metallicity will play a role in the internal structure of M-stars. To investigate this possibility, we plot in Figure 5 the fractional deviation from the [M/H]=0 model prediction as a function of metallicity. The metallicities for most stars are taken from Bonfils et al. (2005) except for those for GJ 191, GJ 205, GJ 887 (Woolf & Wallerstein 2005), and GJ 699 (Ségransan et al. 2003). Efforts to derive accurate metallicities for M dwarfs are in the nascent phase at this time, so the metallicity values should be considered preliminary, although the general trends are likely reliable. We see that the observed radii are approximately consistent with predictions among the metal-poor stars, but the radii become larger than predicted as the metallicity increases. The same conclusion can be drawn from the results of Leggett et al. (2000) who show that the radii derived from spectral fits are systematically larger among stars with higher metallicity when plotted in a ($T_{\rm eff}, R$) diagram (see their Fig. 13). Because metallicity is closely related to stellar opacity, we suspect that the current generation of models for the interiors and atmospheres of M-stars is missing some opacity component that results in larger radii for stars of higher metallicity. We are planning to expand this investigation to other targets with a wider range in metallicity in order to explore this connection further. This work will include more spatial coverage via different baselines and observations at shorter wavelengths to obtain measurements farther along the visibility curves.

We would like to thank PJ Goldfinger, Mandy Henderson, Steve Golden, and Bob Cadman for their tireless efforts at the Array. Construction funding for the CHARA Array has been provided by the National Science Foundation through grant AST 94-14449, the W. M. Keck Foundation, the David and Lucile Packard Foundation, and by Georgia State University. Science operations at the Array are supported by the National Science Foundation through NSF Grant AST-0307562 and by Georgia State University through the College of Arts and Sciences and the Office of the Vice President for Research. Financial support for DHB was provided by the National Science Foundation through grant AST–0205297. This research has made use of the SIMBAD and VizieR (Ochsenbein et al. 2000) databases, operated at CDS, Strasbourg, France. This publication made use of data products from the Two Micron All Sky Survey, which is a joint project of the University of Massachusetts and the Infrared Processing and Analysis Center/California Institute of Technology, funded by the National Aeronautics and Space Administration and the National Science Foundation.

REFERENCES

Andersen, J. 1991, A&A Rev., 3, 91

Balega, I. I., Balega, Y. Y., Maksimov, A. F., Pluzhnik, E. A., Shkhagosheva, Z. U., & Vasyuk, V. A. 1999, A&AS, 140, 287

Baraffe, I., Chabrier, G., Allard, F., & Hauschildt, P. H. 1998, A&A, 337, 403

Benson, J. A., Dyck, H. M., & Howell, R. R. 1995, Appl. Opt., 34, 51

Bidelman, W. P. 1957, PASP, 69, 147

Blackwell, D. E., & Shallis, M. J. 1977, MNRAS, 180, 177

Bonfils, X., Delfosse, X., Udry, S., Santos, N. C., Forveille, T., & Ségransan, D. 2005, A&A, 442, 635

Brott, I., & Hauschildt, P. H. 2005, in The Three-Dimensional Universe with Gaia (ESA SP-576), ed. C. Turon, K. S. O'Flaherty, & M. A. C. Perryman (Noordwijk: ESA), 565 (http://www.rssd.esa.int/index.php?project=Gaia&page=Gaia_2004_Proceedings)

Chabrier, G., & Baraffe, I. 1997, A&A, 327, 1039

Claret, A. 2000, A&A, 363, 1081

Cohen, M., Wheaton, W. A., & Megeath, S. T. 2003, AJ, 126, 1090

Costa, E., Méndez, R. A., Jao, W.-C., Henry, T. J., Subasavage, J. P., Brown, M. A., Ianna, P. A., & Bartlett, J. 2005, AJ, 130, 337

Coudé du Foresto, V., Ridgway, S., & Mariotti, J.-M. 1997, A&AS, 121, 379

Coudé du Foresto, V., et al. 2003, Proc. SPIE, 4838, 280

Cowley, A. P., Hiltner, W. A., & Witt, A. N. 1967, AJ, 72, 1334

Creevey, O. L., et al. 2005, ApJ, 625, L127

Cutri, R. M., et al. 2003, The 2MASS All-Sky Catalog of Point Sources (Pasadena: IPAC/California Inst. Technology) (VizieR on-line catalog II/246)

Davis, J., Tango, W. J., & Booth, A. J. 2000, MNRAS, 318, 387

Delfosse, X., Forveille, T., Mayor, M., Burnet, M., & Perrier, C. 1999, A&A, 341, L63

Delfosse, X., Forveille, T., Perrier, C., & Mayor, M. 1998, A&A, 331, 581

Delfosse, X., Forveille, T., Ségransan, D., Beuzit, J.-L., Udry, S., Perrier, C., & Mayor, M. 2000, A&A, 364, 217

Gizis, J. E., Reid, I. N., & Hawley, S. L. 2002, AJ, 123, 3356

Gliese, W., & Jahreiß, H. 1991, Preliminary Version of the Third Catalogue of Nearby Stars (Heidelberg: Astron. Rechen-Institut.) (VizieR on-line catalog V/70A)

Gray, D. F. 1967, ApJ, 149, 317

Gray, R. O., Napier, M. G., & Winkler, L. I. 2001, AJ, 121, 2148

Hambly, N. C., Henry, T. J., Subasavage, J. P., Brown, M. A., & Jao, W.-C. 2004, AJ, 128, 437

Harlan, E. A. 1969, AJ, 74, 916

Henry, T. J., Ianna, P. A., Kirkpatrick, J. D., & Jahreiss, H. 1997, AJ, 114, 388

Henry, T. J., Kirkpatrick, J. D., & Simons, D. A. 1994, AJ, 108, 1437

Hünsch, M., Schmitt, J. H. M. M., Sterzik, M. F., & Voges, W. 1999, A&AS, 135, 319

Jao, W.-C., Henry, T. J., Subasavage, J. P., Brown, M. A., Ianna, P. A., Bartlett, J. L., Costa, E., & Méndez, R. A. 2005, AJ, 129, 1954

Kurucz, R. L. 1992, in The Stellar Populations of Galaxies: Proc. IAU Symp. 149, ed. B. Barbuy & A. Renzini (Dordrecht: Kluwer Acad.), 225

Lacy, C. H. 1977, ApJ, 218, 444

Lane, B. F., Boden, A. F., & Kulkarni, S. R. 2001, ApJ, 551, L81

Leggett, S. K. 1992, ApJS, 82, 351

Leggett, S. K., Allard, F., Dahn, C., Hauschildt, P. H., Kerr, T. H., & Rayner, J. 2000, ApJ, 535, 965

Leinert, C., Henry, T., Glindemann, A., & McCarthy, D. W. 1997, A&A, 325, 159

Lépine, S. 2005, AJ, 130, 1680

López-Morales, M., & Ribas, I. 2005, ApJ, 631, 1120

Luyten, W. J. 1979, Catalogue of stars with proper motions exceeding 0″.5 annually (Minneapolis: Univ. of Minnesota)

Maceroni, C., & Montalbán, J. 2004, A&A, 426, 577

Maxted, P. F. L., Marsh, T. R., Morales-Rueda, L., Barstow, M. A., Dobbie, P. D., Schreiber, M. R., Dhillon, V. S., & Brinkworth, C. S. 2004, MNRAS, 355, 1143

Mérand, A., Bordé, P., & Coudé du Foresto, V. 2005, A&A, 433, 1155

McAlister, H. A., Hartkopf, W. I., Hutter, D. J., & Franz, O. G. 1987, AJ, 93, 688

McAlister, H. A., et al. 2005, ApJ, 628, 439

Metcalfe, T. S., Mathieu, R. D., Latham, D. W., & Torres, G. 1996, ApJ, 456, 356

Mullan, D. J., & MacDonald, J. 2001, ApJ, 559, 353

Nidever, D. L., Marcy, G. W., Butler, R. P., Fischer, D. A., & Vogt, S. S. 2002, ApJS, 141, 503

Nordstrom, B., et al. 2004, A&A, 418, 989 (VizieR on-line catalog V/117)

Ochsenbein, F., Bauer, P., & Marcout, J. 2000, A&AS, 143, 23

Perrin, G. 2003, A&A, 400, 1173

Perryman, M. A. C., et al. 1997, A&A, 323, L49

Reid, I. N., et al. 2004, AJ, 128, 463

Ribas, I. 2003, A&A, 398, 239

Schmitt, J. H. M. M., Fleming, T. A., & Giampapa, M. S. 1995, ApJ, 450, 392

Ségransan, D., Kervella, P., Forveille, T., & Queloz, D. 2003, A&A, 397, L5

Siess, L., Forestini, M., & Dougados, C. 1997, A&A, 324, 556

Sturmann, J., ten Brummelaar, T. A., Ridgway, S. T., Shure, M. A., Safizadeh, N., Sturmann, L., Turner, N. H., & McAlister, H. A. 2003, Proc. SPIE, 4838, 1208

Subasavage, J. P., Henry, T. J., Hambly, N. C., Brown, M. A., Jao, W.-C., & Finch, C. T. 2005, AJ, 130, 1658

Tango, W. J., & Davis, J. 2002, MNRAS, 333, 642

ten Brummelaar, T. A., et al. 2005, ApJ, 628, 453

Torres, G., & Ribas, I. 2002, ApJ, 567, 1140

van Belle, G. T., & van Belle, G. 2005, PASP, 117, 1263

van Belle, G. T., et al. 2006, ApJ, 637, 494

Woolf, V. M., & Wallerstein, G. 2005, MNRAS, 356, 963

Table 1. Observations

GJ No.	LHS No.	Calibrator Name	Baseline (m)	Date (UT)	No. of Observations
15A	3	HD 2952	W1/E1 (314 m)	2004 Oct 9	2
514	352	HD 119550	S1/E1 (331 m)	2004 Jun 11	4
				2004 Jun 12	4
				2004 Jun 14	6
526	47	HD 119550	S1/E1 (331 m)	2004 Jun 6	3
				2004 Jun 7	1
				2004 Jun 8	1
				2004 Jun 13	5
687	450	HD 151541	S1/E1 (331 m)	2004 Jun 26	5
752A	473	HD 182101	S1/E1 (331 m)	2004 Jun 5	2
				2004 Jun 6	4
				2004 Jun 8	2
				2004 Jun 11	7
				2004 Jun 12	3
				2004 Jun 13	10
				2004 Jun 14	8
880	533	HD 218261	S2/W1 (249 m)	2003 Dec 16	5

Table 2. Calibrators

HD No.	Spectral Classification	$\log(T_{\rm eff})$[a] (K)	[Fe/H][a]	θ_{LD} (mas)	ρ_w	θ_{UD} (mas)
119550	G2 V[b]	3.755	−0.07	0.363 ± 0.015	1.0148	0.358 ± 0.015
151541	K1 V[c]	3.719	−0.36	0.326 ± 0.013	1.0165	0.321 ± 0.013
182101	F6 V[d]	3.799	−0.42	0.367 ± 0.017	1.0120	0.363 ± 0.017
218261	F8.5 V[e]	3.799	0.00	0.387 ± 0.021	1.0139	0.382 ± 0.021

[a]Nordstrom et al. (2004)

[b]Harlan (1969)

[c]Cowley et al. (1967)

[d]Bidelman (1957)

[e]Gray et al. (2001)

Table 3. Calibrated K' Visibilities

Object Name	Date (MJD)	Baseline (m)	Visibility
GJ 15A	53287.364	304.7	0.290 ± 0.013[a]
	53287.390	296.8	0.305 ± 0.021[a]
GJ 514	53167.188	298.3	0.716 ± 0.042
	53167.230	287.8	0.643 ± 0.038
	53167.259	284.8	0.697 ± 0.037
	53167.279	285.0	0.734 ± 0.046
	53168.188	297.4	0.731 ± 0.039
	53168.210	291.4	0.727 ± 0.035
	53168.234	286.7	0.756 ± 0.037
	53168.255	284.8	0.845 ± 0.042
	53170.185	296.7	0.722 ± 0.030
	53170.204	291.5	0.652 ± 0.030
	53170.224	287.5	0.730 ± 0.033
	53170.243	285.2	0.854 ± 0.042
	53170.265	284.7	0.801 ± 0.038
	53170.285	286.4	0.801 ± 0.045
GJ 526	53162.272	297.7	0.688 ± 0.043
	53162.291	297.0	0.702 ± 0.043
	53162.313	298.0	0.672 ± 0.039
	53163.245	300.7	0.645 ± 0.036
	53164.224	304.1	0.569 ± 0.031
	53169.180	311.4	0.555 ± 0.024
	53169.201	306.1	0.637 ± 0.026
	53169.241	298.9	0.734 ± 0.035
	53169.259	297.3	0.734 ± 0.030
	53169.278	297.0	0.691 ± 0.028
GJ 687	53182.186	253.3	0.727 ± 0.041
	53182.200	258.8	0.715 ± 0.044
	53182.213	263.7	0.644 ± 0.041
	53182.227	268.4	0.578 ± 0.035
	53182.241	272.5	0.535 ± 0.033
GJ 752A	53161.452	282.4	0.779 ± 0.040
	53161.470	276.5	0.735 ± 0.036
	53162.405	300.2	0.638 ± 0.041
	53162.433	288.5	0.641 ± 0.035
	53162.449	282.3	0.662 ± 0.041
	53162.468	276.2	0.664 ± 0.042
	53164.449	280.6	0.694 ± 0.044
	53164.462	276.4	0.650 ± 0.042
	53167.359	312.9	0.713 ± 0.043
	53167.376	306.6	0.618 ± 0.035
	53167.391	300.1	0.711 ± 0.038
	53167.411	291.9	0.704 ± 0.043
	53167.424	286.8	0.680 ± 0.052
	53167.437	281.8	0.726 ± 0.053

Table 3—Continued

Object Name	Date (MJD)	Baseline (m)	Visibility
	53167.457	275.4	0.713 ± 0.047
	53168.332	321.3	0.599 ± 0.063
	53168.400	295.2	0.650 ± 0.042
	53168.421	286.8	0.751 ± 0.056
	53169.313	325.4	0.580 ± 0.030
	53169.326	322.1	0.609 ± 0.035
	53169.339	318.0	0.503 ± 0.032
	53169.352	313.7	0.635 ± 0.040
	53169.366	308.3	0.666 ± 0.041
	53169.381	301.9	0.572 ± 0.040
	53169.396	295.7	0.692 ± 0.041
	53169.410	290.2	0.689 ± 0.040
	53169.424	284.7	0.731 ± 0.042
	53169.436	280.3	0.649 ± 0.043
	53170.322	322.4	0.646 ± 0.033
	53170.338	317.7	0.672 ± 0.034
	53170.352	312.7	0.628 ± 0.032
	53170.372	304.9	0.662 ± 0.032
	53170.384	299.7	0.760 ± 0.040
	53170.399	293.6	0.629 ± 0.039
	53170.412	288.1	0.682 ± 0.044
	53170.425	283.3	0.734 ± 0.044
GJ 880	52928.301	247.4	0.727 ± 0.024
	52928.315	244.7	0.716 ± 0.026
	52928.326	241.7	0.731 ± 0.024
	52928.334	238.9	0.718 ± 0.022
	52928.351	231.7	0.698 ± 0.025

[a]Visibilities are given as $\mathcal{V}^2$

Table 4. Derived Stellar Parameters

Object Name	θ_{UD} (mas)	θ_{LD} (mas)	$\chi^2_{\rm red}$	$\log L_{bol}$ (erg s^{-1})	Radius ($R_\odot$)	$T_{\rm eff}$(BC) (K)	$T_{\rm eff}$(2MASS) (K)	$\log g$ (cm s^{-2})
GJ 15A	0.976 ± 0.016	0.988 ± 0.016	0.06	31.99	0.379 ± 0.006	3747	3730 ± 49	4.89
GJ 514	0.740 ± 0.044	0.753 ± 0.052	2.50	32.22	0.611 ± 0.043	3377	3243 ± 160	4.59
GJ 526	0.830 ± 0.050	0.845 ± 0.057	3.41	32.18	0.493 ± 0.033	3662	3636 ± 163	4.75
GJ 687	0.990 ± 0.059	1.009 ± 0.077	3.06	31.91	0.492 ± 0.038	3142	3095 ± 107	4.66
GJ 752A	0.822 ± 0.049	0.836 ± 0.051	1.49	32.10	0.526 ± 0.032	3390	3368 ± 137	4.68
GJ 880	0.918 ± 0.055	0.934 ± 0.059	0.92	32.32	0.689 ± 0.044	3373	3277 ± 93	4.53

Table 5. Adopted Stellar Parameters

Object Name	Spectral Classification[a]	[Fe/H][b]	Mass[c] ($\mathcal{M}_\odot$)	Parallax[d] (arcsec)
GJ 15A	M1.5 V	−0.46	0.404	0.28059 ± 0.00095
GJ 514	M1.0 V	−0.27	0.526	0.13257 ± 0.00118
GJ 526	M1.5 V	−0.31	0.502	0.18421 ± 0.00116
GJ 687	M3.0 V	+0.11	0.401	0.22049 ± 0.00082
GJ 752A	M3.0 V	−0.05	0.484	0.17101 ± 0.00062
GJ 880	M1.5 V	−0.04	0.586	0.14579 ± 0.00113

[a]From Henry et al. (1994).

[b]From Bonfils et al. (2005). The typical error in [Fe/H] is ±0.2 dex.

[c]From Delfosse et al. (2000) and we adopted a 10% error in mass

[d]NStars database, http://nstars.nau.edu

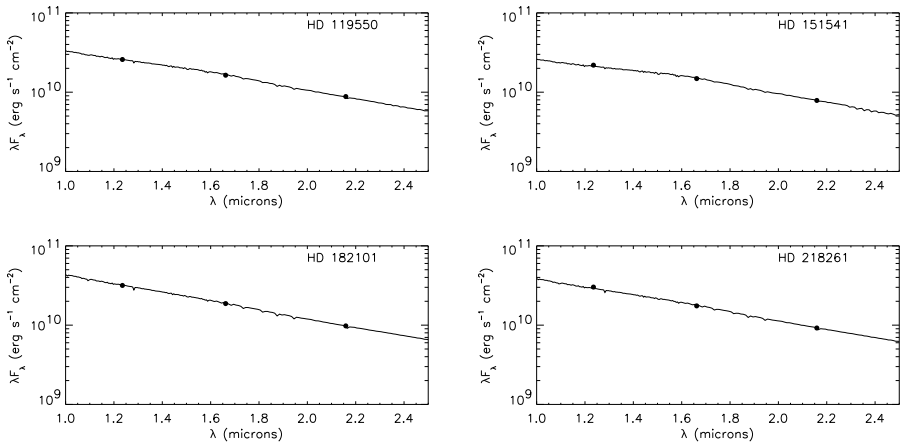

Fig. 1.— Spectral energy distribution fits used to derive the calibrator angular diameters from the IRF method. The model atmosphere fluxes (Kurucz 1992) are shown as a solid line, and the filled circles give the observed fluxes from the 2MASS J, H, K photometry (Cutri et al. 2003; Cohen et al. 2003). The errors in the 2MASS fluxes are approximately $\pm 2\%$ (much smaller than the symbol size).

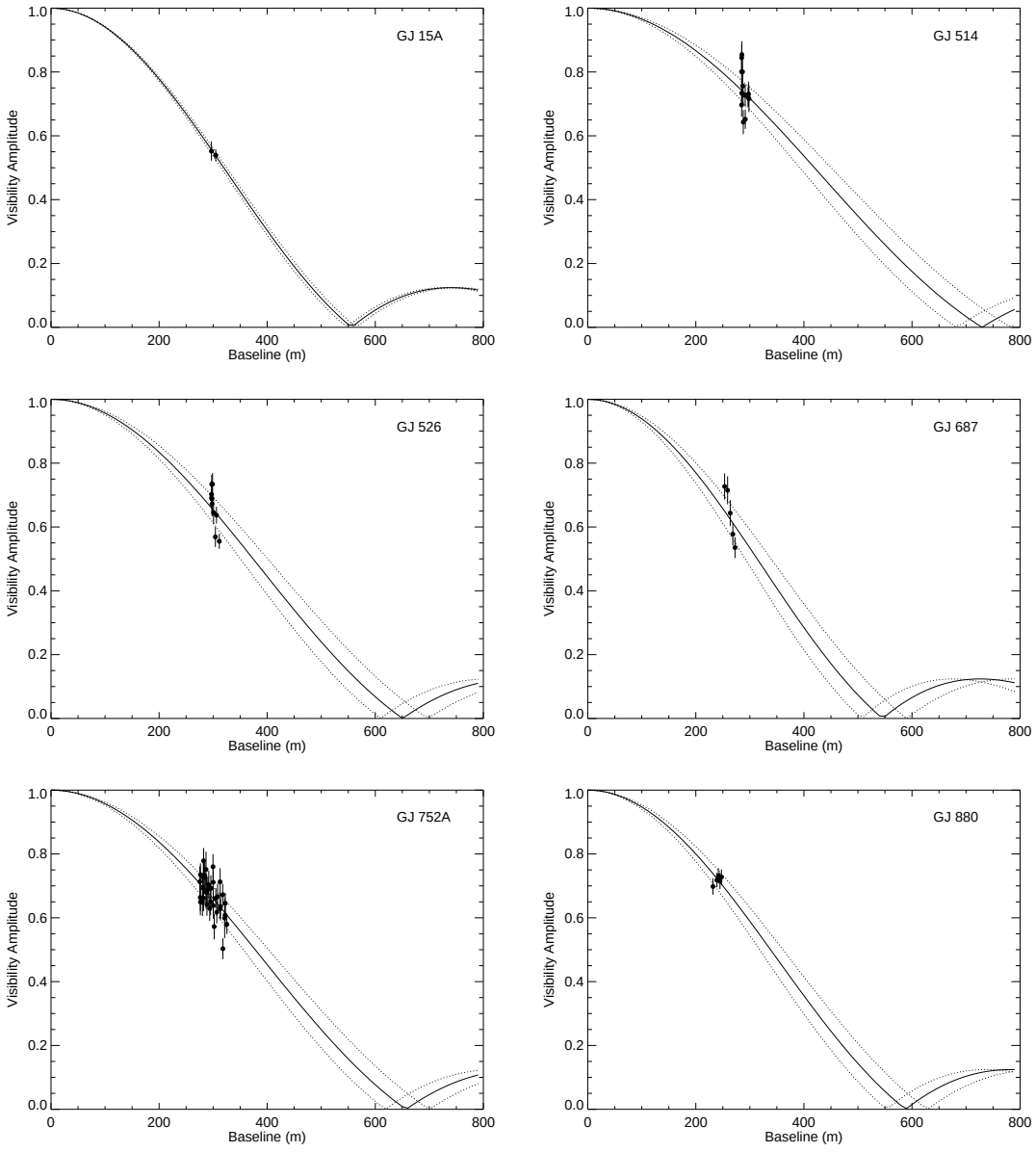

Fig. 2.— Observed visibilities and fitted visibility curve (solid line) for a limb darkened disk (using a K-band limb darkening law from Claret 2000 for the stellar parameters given in Table 4). Dotted lines represent the total error to the model fit.

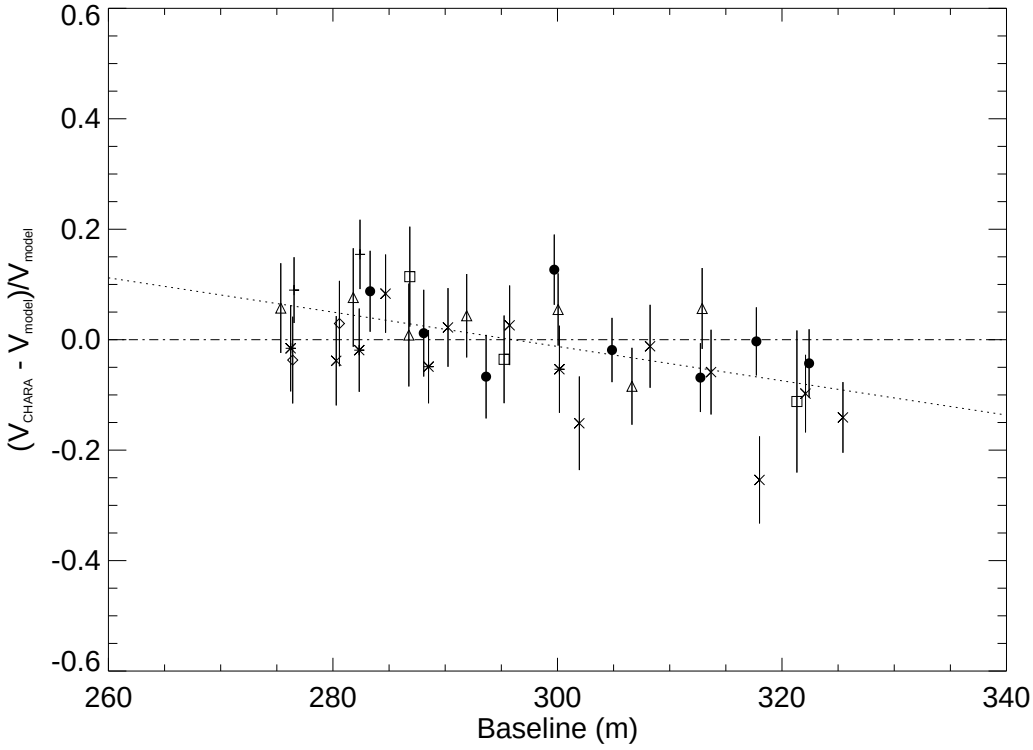

Fig. 3.— Fractional deviation between the observed visibilities and fitted visibility curve for a limb darkened disk (same as in Fig. 2) for GJ 752A. The dotted line represents a best fit regression line. Symbols indicated data taken on different nights ($+$ = 2004 Jun 5, $*$ = 2004 Jun 6, $\diamond$ = 2004 Jun 8, $\triangle$= 2004 Jun 11, $\square$ = 2004 Jun 12, $\times$ = 2004 Jun 13, $\bullet$ = 2004 Jun 14).

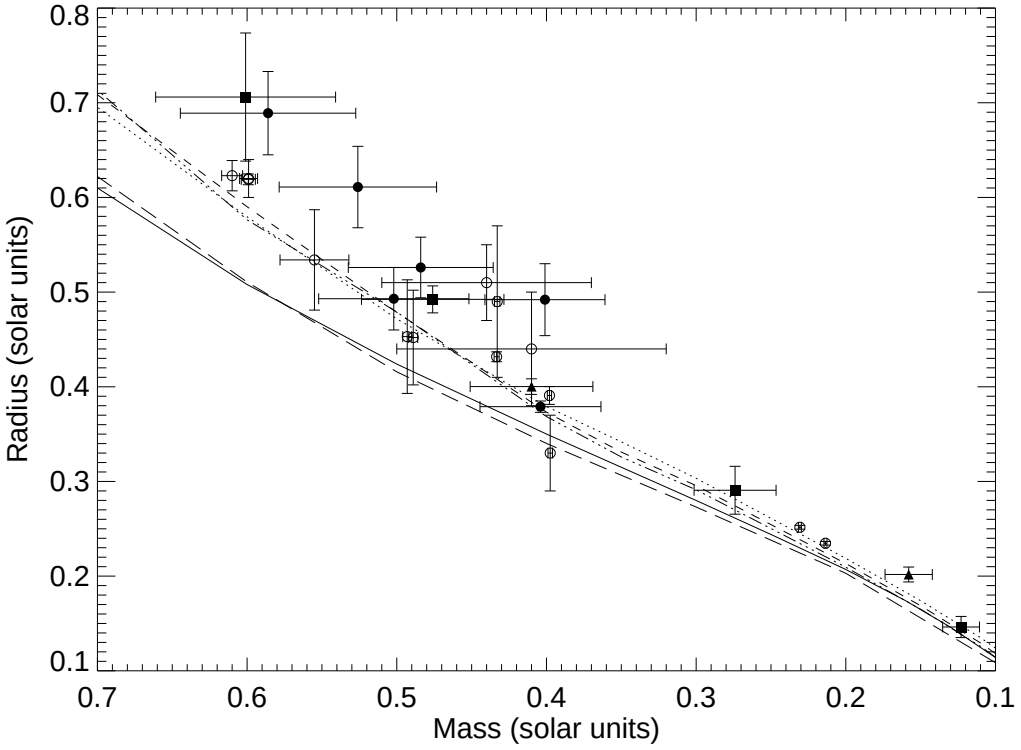

Fig. 4.— The mass–radius relation for low-mass dwarfs measured by long-baseline interferometry (filled symbols) and spectrophotometry of eclipsing binaries (open circles, see references in § 1). The interferometry data included are from this paper (circles), PTI (Lane et al. 2001, triangles), and VLTI (Ségransan et al. 2003, squares). The lines represent models from Chabrier & Baraffe (1997) for different metallicities ($\cdots$ for [M/H]= 0.0; - - - - for [M/H]= -0.5; $-\cdots$ for [M/H]= -1.0) and Siess et al. (1997) for similar metallicities (— for [M/H]= 0.0; – – – for [M/H]= -0.3).

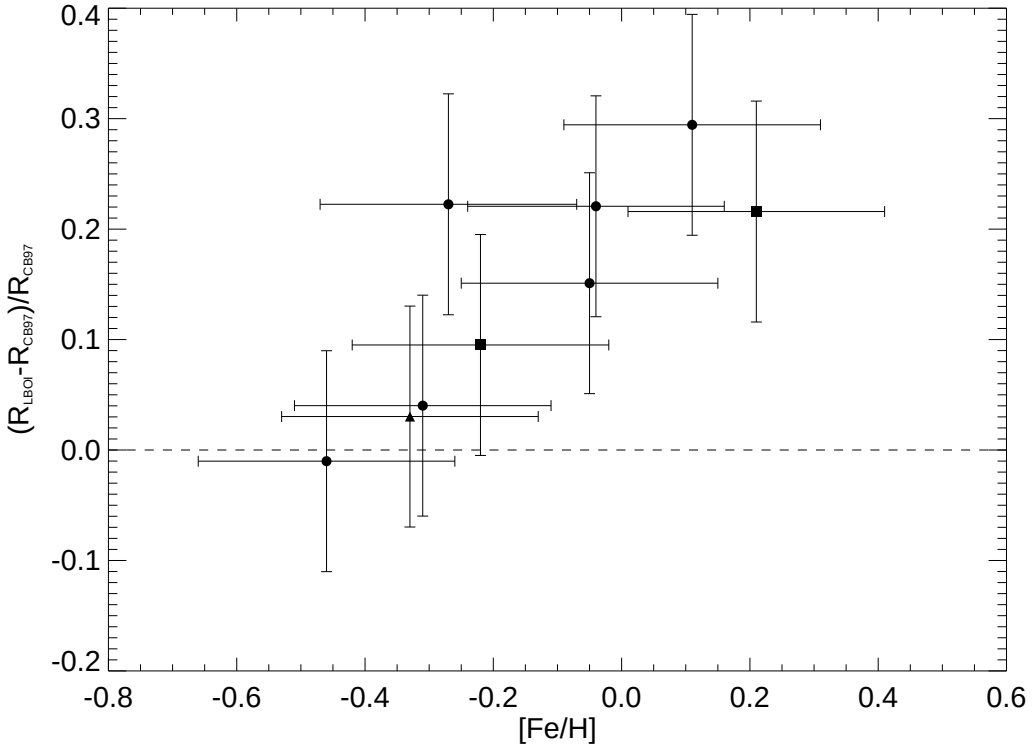

Fig. 5.— Fractional deviation between the radii measured through long baseline optical interferometry (designated LBOI) and from the model predictions for stellar radius from Chabrier & Baraffe (1997, designated CB97) plotted as a function of metallicity. The symbols represent the same observational groups given in Fig. 4. The representative errors are ±0.2 dex in [Fe/H] and ±0.1 in fractional deviation of the radius (due to 10% errors in the mass estimates).